PAPER

Check for updates

Numbering up and sizing up gliding arc reactors to enhance the plasma-based synthesis of NOₓ†

Thijs van Raak, [iD][a] Huub van den Bogaard,[a] Giulia De Felice, [iD][a] Daniël Emmery,[a] Fausto Gallucci[ab] and Sirui Li [iD]*[a]

Non-thermal plasma-based NOₓ synthesis from ambient air is receiving an increasing amount of interest for its potential in small-scale, sustainable fertilizer production. Nevertheless, most reported research focuses on lab-scale systems and a single reactor with limited production. In this work, two gliding arc reactors (GARs) with 2 mm discharge gaps were connected in series or in parallel to explore strategies for scaling up the productivity. A single GAR with an enlarged discharge gap of 4 mm was also investigated for comparison. Operation parameters such as flow rate, discharge power & mode, and effective residence time were tested. The NOₓ concentration increased for all configurations with an increase in specific energy input (SEI), and effective residence time. The case of reactors connected in series outperformed all other configurations. The energy consumptions and NOₓ productions achieved were $2.29-2.42$ MJ mol_N^{-1} and $124.6-158.3$ $mmol_N$ h^{-1}, respectively. The NO_2 selectivity could be enhanced by prolonging the post-plasma oxidation time while consuming the excess O_2 in the feed and utilizing the low temperatures at the reactor(s) outlet. By using this connection strategy, NOₓ production can be doubled with a 20.9% improvement in energy consumption compared to a single reactor.

1. Introduction

Synthetic nitrogen fixation is one of the most crucial chemical processes to sustain humanity on Earth. Without this process, food security cannot be ensured due to the importance to the production of synthetic fertilizer.[1,2] The fertilizer production is dominated by the commercialized Haber–Bosch (HB) process.[3] This process requires severe operating conditions, even after more than a century of optimization, which results in a 2% annual energy consumption of the total world's energy supply.[4] Besides, this process releases $1.9-2.3$ ton CO_2/ton NH_3 obtained, mostly caused by the required hydrogen production.[5,6] The Food and Agricultural Organization of the United Nations (FAO) reported a total fertilizer use of 189 Mton in 2019.[7] Despite the large amount of fertilizer that has been produced every year, hunger has grown, with 786 million people suffering from undernourishment in 2021.[8] Moreover, the world's population is continuously growing, generating an even higher demand of fertilizer.[9] To decrease

the environmental footprint of synthetic nitrogen fixation, more sustainable alternatives were explored for the past few decades, and non-thermal plasma is one promising technology that has attracted much attention.[10]

The use of non-thermal plasma (NTP) provides many advantages, and not solely owing to its highly reactive nature.[11] NTP can be created under ambient or mild operation conditions, is suitable for decentralized applications at small scale, and does not require steady-state operation due to fast dynamic control and low temperature of the gas exiting the reactors.[12] It is therefore possible to integrate NTP with renewable energy sources enabling the possibility of sustainable nitrogen fixation.[13] The synthesis of NH_3 by plasma in combination with catalysts has been an interesting topic that has received much attention in recent years. Nevertheless, the direct synthesis of NO_x by plasma has significant potential for applications such as fertilizer and nitric acid production. This approach can circumvent the need for the initial synthesis of NH_3, which is subsequently oxidized to yield NO_x in the conventional thermo-catalytic route. Moreover, ambient air can be directly utilized for NO_x synthesis, thus avoiding further energetically demanding process steps such as air separation to obtain nitrogen, and additional H_2 production. This renders it more suitable for the development of processes targeting decentralized scenarios, especially on small scales.

[a] Sustainable Process Engineering, Department of Chemical Engineering and Chemistry, Eindhoven University of Technology, De Rondom 70, Eindhoven, 5612 AP, The Netherlands. E-mail: s.li1@tue.nl
[b] Eindhoven Institute for Renewable Energy Systems (EIRES), Eindhoven University of Technology, PO Box 513, Eindhoven, 5600 MB, The Netherlands

† Electronic supplementary information (ESI) available. See DOI: https://doi.org/10.1039/d4cy00655k

This journal is © The Royal Society of Chemistry 2024

Catal. Sci. Technol., 2024, **14**, 5405–5421 | **5405**

Many scientists have explored plasma based N-fixation using different types of NTP reactors. Among the most common ones are dielectric barrier discharge (DBD) reactors,[14–17] Microwave (MW) discharges,[18,19] (atmospheric pressure) glow discharges (APGD),[20,21] and gliding arc reactors (GARs).[22–25] Recent research on NO_x synthesis focused on 'warm' plasma including gliding arc reactors since promising results in terms of energy consumption (EC) can be achieved, specifically compared to cold plasma-based literature.[11] Besides, they can be operated at a variety of power levels and flow rates at an ambient pressure working range. GARs generally operate in a range of reduced electric field strengths between 5 and 100 Td, which efficiently targets vibrational excitation of N_2.[13] This type of excitation promotes the energy efficient non-thermal Zeldovich mechanism.[26] This mechanism consists of two subsequent reactions, which are shown in reaction equations (R1) and (R2).[11] The reaction between atomic oxygen and vibrationally-excited nitrogen, N_2 (v), results in the formation of molecular NO and a nitrogen atom, as shown in reaction equation (R1). The N-atom subsequently reacts with molecular oxygen to form another NO molecule and a new O-atom, according to reaction equation (R2).

$$O + N_2(v) \rightarrow NO + N \tag{R1}$$

$$N + O_2 \rightarrow NO + O \tag{R2}$$

Recently published works showed large progress regarding the decrease of EC and increase of production yields. For example, Vervloessem *et al.* obtained an impressive EC of 0.42 MJ mol_N^{-1} in their soft jet reactor using a pulsed plasma; however, only 200 ppms of NO_x were obtained.[27] Van Alphen *et al.* presented a rotating gliding arc (RGA) reactor, coupled it with an effusion nozzle and obtained 5.9 vol% of NO_x at an EC of 2.1 MJ mol_N^{-1}.[22] Changing operational parameters such as pressure could also enhance the process drastically, as recently shown by Tsonev *et al.*[23] The authors increased the operation pressure using a needle valve, which resulted in pressures up to 3 barg. Their production rate rose up to 50 g h^{-1} at a 1.8 MJ mol_N^{-1}. Nevertheless, most reactors were designed for lab-scale applications, and showed limited production. Hence, process optimization and scale up remains a significant technological challenge as suggested in the 2022 Plasma Roadmap.[28] Besides, a high selectivity towards NO_2 is desired, as this is the primary intermediate for the production of fertilizers, as shown in reaction equation (R3).

$$3NO_2(g) + H_2O(l) \rightleftharpoons 2HNO_3 + NO(g) \tag{R3}$$

Two commonly used strategies to scale up the production are numbering-up and sizing-up reactors. Different configurations exist in gas connections and electrical connections in case of reactor numbering up, which results in different process' performances. Therefore, the influence of reactor connection on the overall performance of NO_x production was investigated in this work. It needs to be noted that the purpose of this work is to provide insights on the configuration of reactor connections, which is important for the numbering up strategy when considering scaling up the process. New design or optimization of single reactors could also improve plasma-based NO_x synthesis, but this is not the focus of this work. Accordingly, the well-studied classic 2D-GAR design was used in experiments. Two reactors were installed *via* a gas connection in series or parallel, and a comparison study was conducted using a reactor with double the size. The results, including NO_x concentrations, ECs, and NO_2 selectivities, were analyzed under various operating conditions. Subsequent discussions on differences in discharge mode, power, and effective residence time were provided. Finally, the utilization of employing a catalyst in conjunction with a GAR was discussed, with particular attention devoted to the prospective use of a post-plasma catalyst to guarantee the highest selectivity towards NO_2 production.

2. Experimental

The set-up schematic is shown in Fig. 1(a). Compressed dry air (CDA) was used as feed gas. The volumetric feed flow rate (F_{v0}) was regulated by a Bronkhorst mass flow controller, calibrated at 1.013 bar and 0 °C. CDA was fed to the reactor at a flow rate ranging from 1 to 5 L min^{-1}. All the experiments were conducted without external pressure or temperature modulation. A single reactor is pictured in Fig. 1(b). The inner part of every GAR contained two 1.00 mm thick, diverging, tungsten electrodes, at an angle of 75° with respect to the horizontal. The electrodes were enclosed with two 6 mm thick quartz plates inserted in a PEEK frame. Consequently, the arc could only propagate in the longitudinal direction, hence the name 2D-GAR. The total height of the PEEK frame was 15.4 cm.

The average volume covered by plasma was estimated using images as shown in Fig. 1(b), taken by a Sony® FDR-AX33 Digital 4K video camera recorder at a 4288 × 2408 resolution. The shutter speed was set at 167 ms. This volume was assumed to be a trapezoid with a thickness of 1.00 mm, and a maximum height *H*. The number of pixels on the 15.4 cm line was used as a reference to convert the number of pixels to centimeters. The plasma volume was calculated based on the height and the geometry of the reactor using eqn (1). More details can be found in section SI.1 of the ESI.† And the effective residence times were calculated using eqn (2).

$$V_{plasma}(mm^3) = d_{gap}H \cdot 1.00 + \tan(0.2618)H^2 \cdot 1.00 \tag{1}$$

5406 | *Catal. Sci. Technol.*, 2024, **14**, 5405–5421

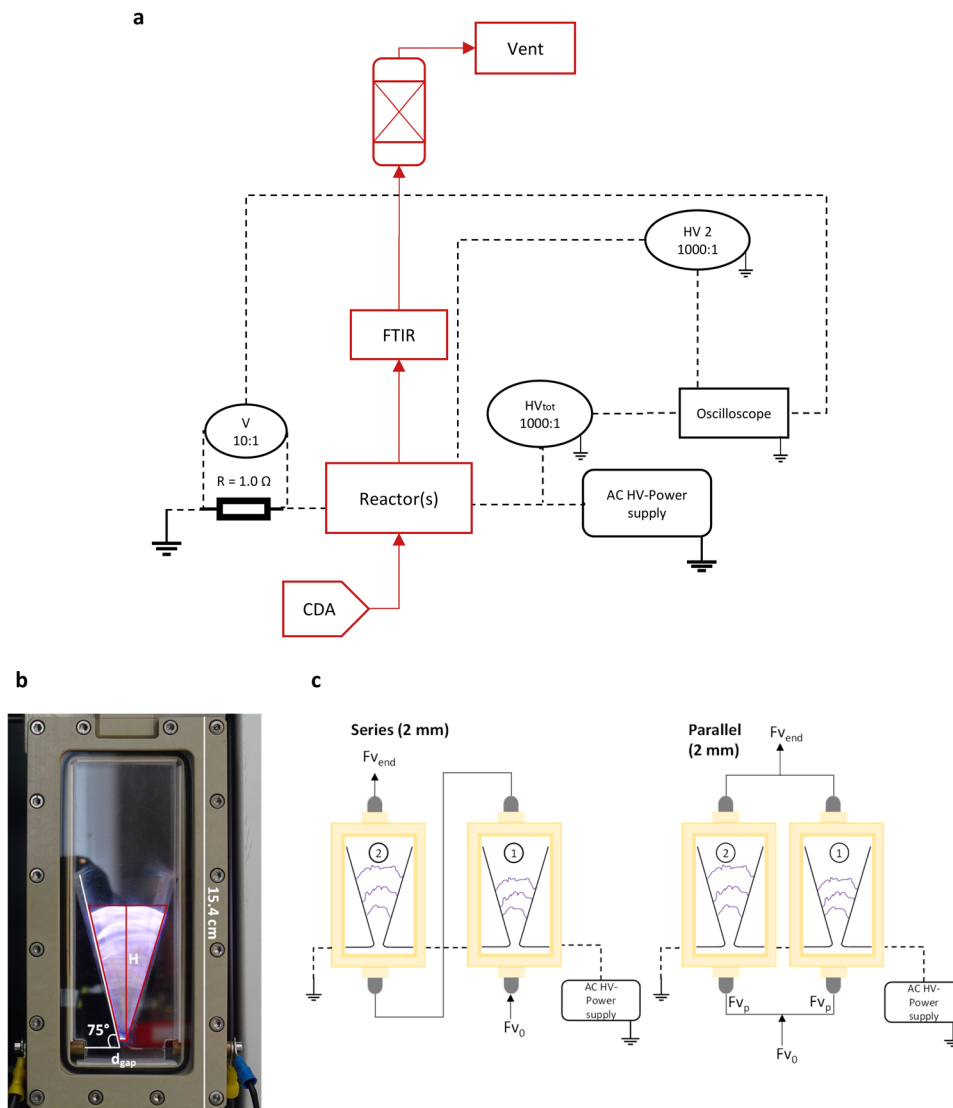This journal is © The Royal Society of Chemistry 2024

Fig. 1 (a) Experimental set-up schematic. (b) A single GAR with a 2 mm discharge gap. The trapezoid surface in red represents the plasma volume at a flow rate of 1 L min^{-1} CDA. (c) Schematics of the series and parallel topology, including gas (solid) and electrical (dashed) connections.

$$\tau(\text{ms}) = \frac{V_{\text{plasma}}(\text{mm}^3)\cdot 10^{-3}\cdot 60\left(\text{s min}^{-1}\right)}{F_{v0}\left(\text{L min}^{-1}\right)} \qquad (2)$$

To study the numbering up strategy, two identical GARs were connected in series or parallel as shown in Fig. 1(c). The narrowest discharge gap of the reactor is 2 mm, hence it is referred as the 2 mm reactor in this paper. In order to distinguish between the two GARs, labels 1 and 2 were assigned. Reactor 1 was the GAR directly connected to the high-voltage power supply, while reactor 2 was connected between reactor 1 and the ground. Note that in both series and parallel case, the reactors are electrically connected in series. The terms "series" and "parallel" refer to the gas line connection of the reactor. The feed flow rate in the parallel topology was ideally equally divided in split fractions F_{vp}, due to an inserted T-piece. To verify that the flows were split equally, a Horiba-stec VP4 flowmeter was installed. An average deviation of 9.5% was observed depending on the feed flow rate. As a benchmark case, experiments were also conducted with one single reactor. Furthermore, one reactor with a discharge gap twice the size (4 mm at the narrowest gap, referred as 4 mm reactor) was also studied for comparison.

The outlet of the reactors led to a Shimadzu IRTracer-100 Fourier transformer infrared spectrometer (FTIR), which was equipped with a gas cell containing a Harrick BaF$_2$ window. The temperature and pressure of the FTIR inlet were measured with a pressure indicator (Dresser Instruments) and a K-type thermocouple, respectively. The FTIR was used to determine the concentrations of NO$_x$ products. The FTIR spectra only indicated peaks corresponding to NO, NO$_2$, and N$_2$O$_4$. The observed N$_2$O$_4$ peaks were identified at the

This journal is © The Royal Society of Chemistry 2024

Catal. Sci. Technol., 2024, **14**, 5405–5421 | **5407**

wavenumbers 1260 and 1743 cm^{-1}, indicating the formation of N$_2$O$_4$ due to the dimerization of NO$_2$, as shown in reaction equation (R4). The reversible dimerization reaction of NO$_2$ is exergonic, favorable at low temperatures and equilibrium is established rapidly.[29,30] In this work NO$_x$ refers to all three obtained reactive nitrogen derivatives, thus including N$_2$O$_4$. Besides, it is possible that irreversible NO oxidation may also occur as a consequence of post-plasma oxidation in the tubing that connects the outlet of the reactors with the FTIR inlet, as indicated in reaction equation (R5). To mitigate this effect, the minimum internal volume of tubing was installed, resulting in a volume of 0.13 L. It is unavoidable that a certain amount of tubing must be used to connect the GAR outlet due to the potential for electromagnetic interference induced by the GAR(s), which could result in alterations to the accuracy of the FTIR. Consequently, the NO or NO$_2$ concentration directly at the GAR system's outlet can only be estimated based on back-calculations from the measured values. Therefore chemical kinetic calculations were conducted, which are further explained in section 3.4.

The determined concentrations in mol L^{-1} were inserted in eqn (3) to calculate the overall NO$_2$ selectivity. Moreover, every measured FTIR spectrum contained an average of 10 scans with a 0.4 cm^{-1} resolution obtained in one minute. Multiple spectra were measured simultaneously with their corresponding discharge powers. A priorly constructed calibration curve was prepared at 20 °C using LabSolutions software. This curve was used to quantify the obtained NO$_x$ concentration (C$_{NO_x}$) for every spectrum. The averages of the quantified C$_{NO_x}$ and discharge powers were taken.

$$2NO_2 \rightleftharpoons N_2O_4 \qquad (R4)$$

$$2NO + O_2 \rightarrow 2NO_2 \qquad (R5)$$

$$S_{NO_2}(\%) = \frac{[NO_2]}{[NO] + [NO_2] + 2 \cdot [N_2O_4]} \cdot 100\% \qquad (3)$$

An AC high voltage power supply (AFS G05F) was used for plasma generation. The supplied voltage was set to a frequency of 8.0 kHz and a duty cycle of 95%. A 1.0 Ω resistor was connected in the circuit, and the total discharge current was determined by Ohm's law based on the voltage across this resistor, which was measured by a 10:1 voltage probe (Pico Technology TA150). The total voltage delivered to the reactors was measured with a 1000:1 HV-probe (Tektronix P6015A), represented as HV$_{tot}$. In case of two reactors, a second HV-probe (HV$_2$) was installed to measure the voltage across the second reactor. HV$_1$ was then calculated by subtracting HV$_2$ from HV$_{tot}$. All three voltage probes were connected to a 5 Gs s^{-1} oscilloscope (PicoScope 6402D), which enabled recording of all three waveforms to calculate the discharge power.

The supplied discharge power P_i was calculated by integrating the voltage U_i, and current I waveforms for every full envelope time T_{env}, with eqn (4). The envelope time is the total time between arc ignition to extinguishment. The subscript i was used to distinguish between GAR 1 and 2 according to the labels in Fig. 1(c). Other parameters used throughout this study were specific energy input (SEI) and energy consumption (EC), which were calculated using eqn (5) and (6), respectively. V_m is the molar volume, F_v the volumetric flow rate at the reactor outlet and y_{N_r} the volumetric fraction of every reactive form of nitrogen.

$$P_i(W) = \frac{1}{T_{env(ms)}} \int_0^{T_{env}} U_i(V) \cdot I(A) dt \qquad (4)$$

$$SEI(kJ\ L^{-1}) = \frac{P(W) \cdot 10^{-3} \cdot 60(s\ min^{-1})}{F_{v0}(L\ min^{-1})} \qquad (5)$$

$$EC(MJ\ mol_N^{-1}) = \frac{P(W) \cdot 10^{-6}}{F_{N_r}(mol_N\ s^{-1})}$$
$$= \frac{P(W) \cdot 60(s\ min^{-1}) \cdot V_m(L\ mol^{-1}) \cdot 10^{-6}}{F_v(L\ min^{-1}) \cdot y_{N_r}} \qquad (6)$$

3. Results & discussion

3.1 Series and parallel topology

The first experiments were conducted with reactors connected in series and parallel by varying volumetric feed flow rates. The minimum flow of 1 L min^{-1} fed to the parallel system resulted in a static arc and was therefore excluded from this comparison. The discharge power for the topologies under different flow rates were calculated and the results are shown in Fig. 2. The total power of the system with parallel-connected reactors was not significantly influenced by the changes in feed flow rate and the values were in a range between 98.33–106.30 W. In the case of the system with series-connected reactors, the total discharge
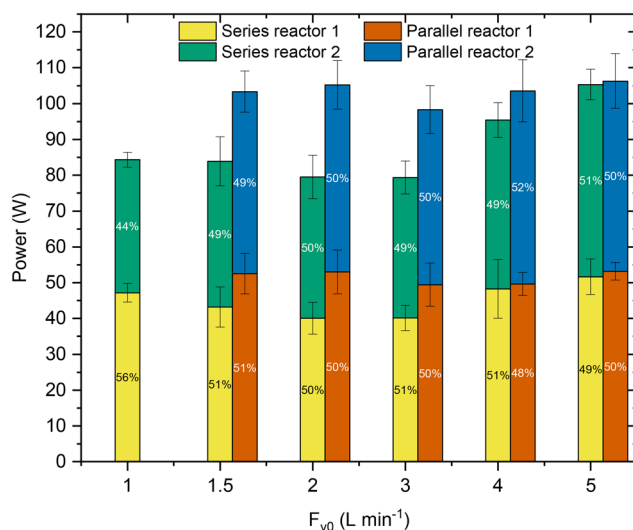

Fig. 2 Supplied power as function of different flow rates for GARs connected in series and parallel.

5408 | *Catal. Sci. Technol.*, 2024, **14**, 5405–5421

This journal is © The Royal Society of Chemistry 2024

power is generally lower than the case of the parallel system, especially under the flow rate of 3 L min^{-1} or below. However, as the flow rate increased to 4 L min^{-1} and above, a higher power output was achieved, resulting in comparable values to those observed in the parallel system. Furthermore, Fig. 2 also shows the power distribution among individual reactors as a percentage. In most of the tests, power was nearly evenly distributed, except for the series system operating at 1 L min^{-1}. Notably, in this particular experiment with the lowest flow rate tested, the voltage across the first reactor continuously exceeded the voltage of the second reactor throughout the entire envelope. The difference is relevant to the complex dynamics of the arc and circuit impedance which requires more in-depth study in the future. Additional details are shown in Fig. SI.2.1 in the ESI.†

The plasma volumes, and corresponding fractions per reactor as function of flow rate were determined, and the results are shown in Fig. 3(a). In the case of the system with series-connected reactors, the total volume consistently remained larger than for the system with parallel-connected reactors and increased with increasing flow rate to a peak value of 1.736 cm^3 at 3 L min^{-1}, followed by a decline at higher flow rates. Conversely, for the parallel system, the volume is lower and it continued to increase with flow rate until 5 L min^{-1}, up to a maximum of 1.228 cm^3. From the volume, the effective residence time, τ (ms), was calculated by eqn (2), and the results as function of flow rate are shown in Fig. 3(b). A decrease in effective residence time was observed, when the flow rate increased for both series and parallel systems. The effective residence time of the series system always exceeded the effective residence time of the parallel system for every applied flow rate, which was expected due to the enhanced plasma volumes of series compared to parallel system. However, the absolute difference in effective residence time between the two configurations decreased

when the flow rate increased, reaching 18.505 ms at 1.5 L min^{-1} and 0.373 ms at 5 L min^{-1}.

It also can be seen from Fig. 2 and 3 that the flow rate, power and plasma volume are correlated, and one parameter cannot be varied without changing the other. Furthermore, a GAR can be regarded as a dynamic load in the circuit. Since two GARs were connected, the complexity of the analysis of the circuit, and voltage–current characteristics largely increased. Nevertheless, examples of voltage and current waveform for the system with series- and parallel-connected reactors at a feed flow rate of 1.5 L min^{-1} are shown in Fig. 4(a) and (b), respectively. The measured voltage exhibited typical envelope behavior corresponding to the development of the gliding arc from ignition to extinguishment. The durations for one envelope, T_{env}, are indicated in the figure along with the ignition (t_1) and extinguishment (t_2) time. HV$_1$ and HV$_2$ are the high voltages across the first and second reactor, respectively. Fig. 4 show differences in envelope times between HV$_1$ and HV$_2$ in both reactor configurations. Generally, the envelope times of HV$_2$ exceeded the envelope times of HV$_1$. However, occasionally an equal envelope time was observed. This is also reflected in Fig. 3(a), where the plasma volume of reactor 2 always exceeded that of reactor 1, since the length of the envelope time corresponds to the time for the arc to glide towards the higher zone of the reactor, which is accompanied by an increased plasma volume.

The average total envelope times as function of flow rates for both reactor configurations are shown in Table 1. The envelope time decreased with an increase in flow rate for both systems with series- or parallel-connected reactors. The shorter envelope time at higher flow rate was likely a result of the enhanced convective transport, which facilitated the arc extinguishment. This transport resulted in a more rapid dissipation of charged species, which were needed to maintain arc stability.[31,32] The deficiency of charged species
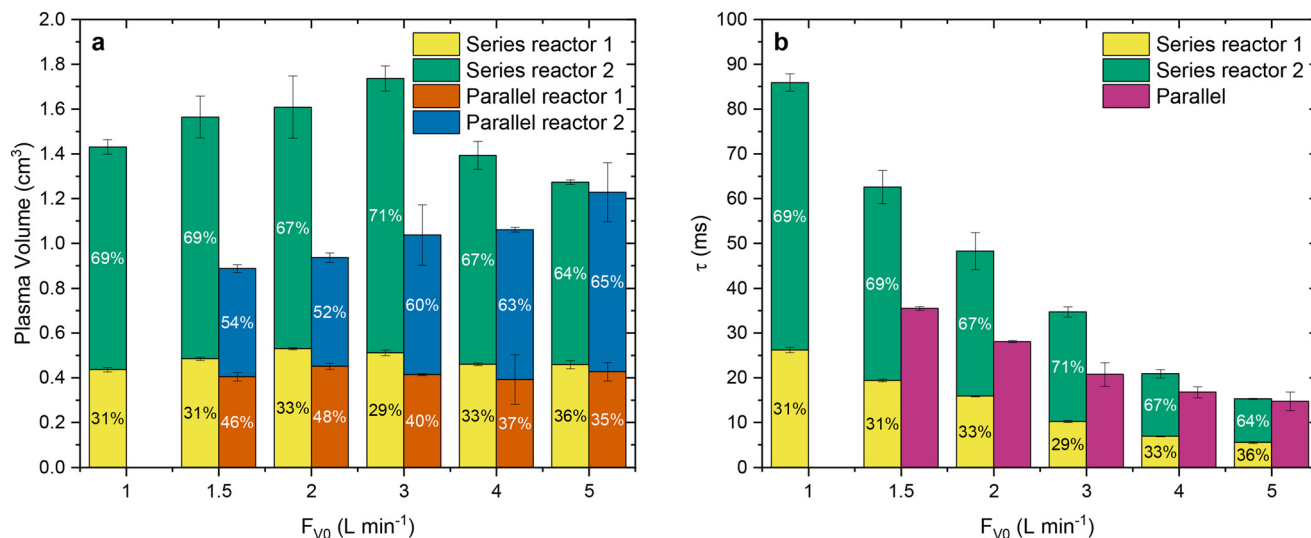

Fig. 3 (a) Plasma volume and (b) effective residence time as function of flow rate for reactors connected in series and parallel.
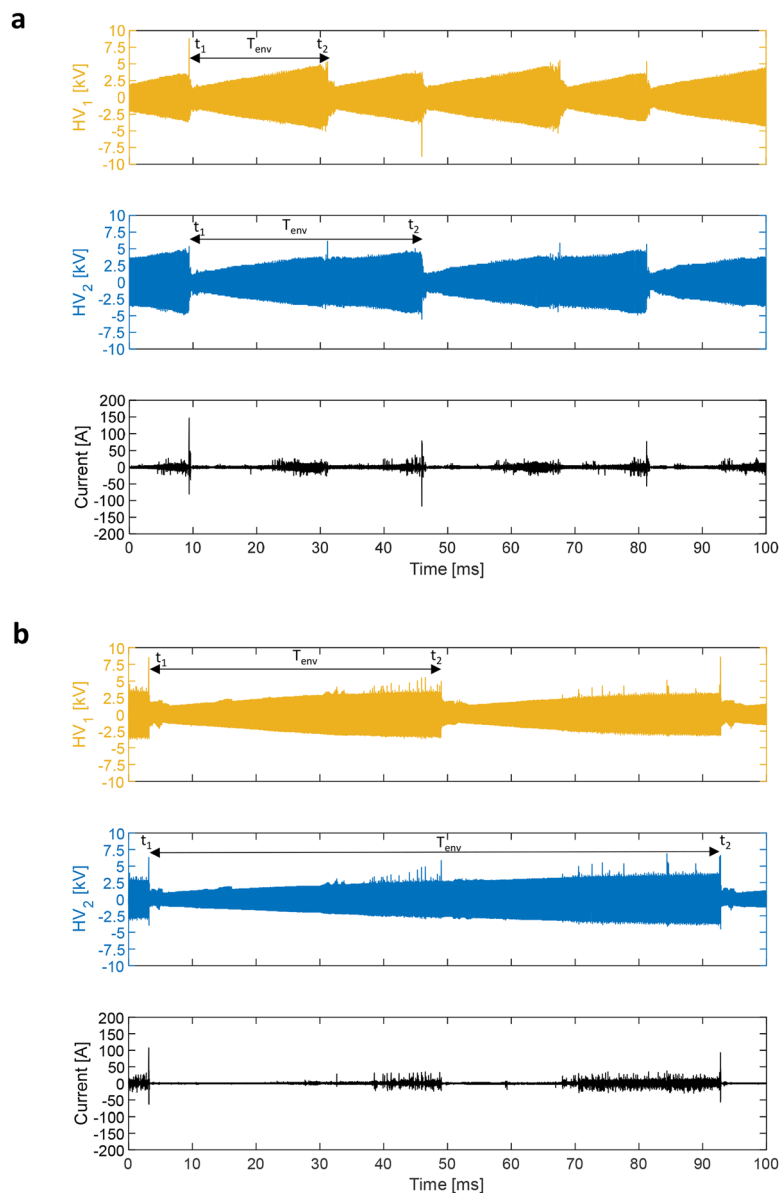
Fig. 4 (a) Voltage and current plots at a 1.5 L min^{-1} feed flow rate for reactors connected in series and (b) parallel.

resulted in arc extinguishment, then reignition occurred to start a new cycle.[33] Furthermore, the envelope time of the system with parallel-connected reactors exceeded the one of the system with series-connected reactors at equal flow rates. This difference was mainly caused by the 50%

Table 1 Envelope times for the system with series- and parallel-connected reactors

F_{v0} (L min^{-1})	$T_{env,series}$ (ms)	$T_{env,parallel}$ (ms)
1	48.45 ± 8.65	—
1.5	25.97 ± 6.30	78.60 ± 12.36
2	14.58 ± 3.61	65.43 ± 24.62
3	8.21 ± 0.73	27.70 ± 5.21
4	5.64 ± 0.44	22.88 ± 7.40
5	4.29 ± 0.68	13.90 ± 8.03

split fraction of feed flow rate in the parallel system, which subsequently decreased the superficial gas velocity and arc propagation velocity, leading to a longer arc gliding cycle.

Fig. 4(a) and (b) show differences in current profiles for both reactor configurations. Current peaks were observed at the onset of each envelope, which corresponds to the ignition stage of the gliding arc, indicating a spark-like discharge behavior. In addition, near the end of every envelope shown in HV$_1$ or HV$_2$, the current increased, which was also observed by our previous work and the work of Zhang *et al.*[25,34] Since the envelope time is longer in the case of the system with parallel-connected reactors, the reignition and extinguishment of the GA is less frequent, hence fewer peaks above several amperes were measured. Furthermore, as the envelope time decreased with the increase in flow rate, it can

5410 | *Catal. Sci. Technol.*, 2024, **14**, 5405–5421

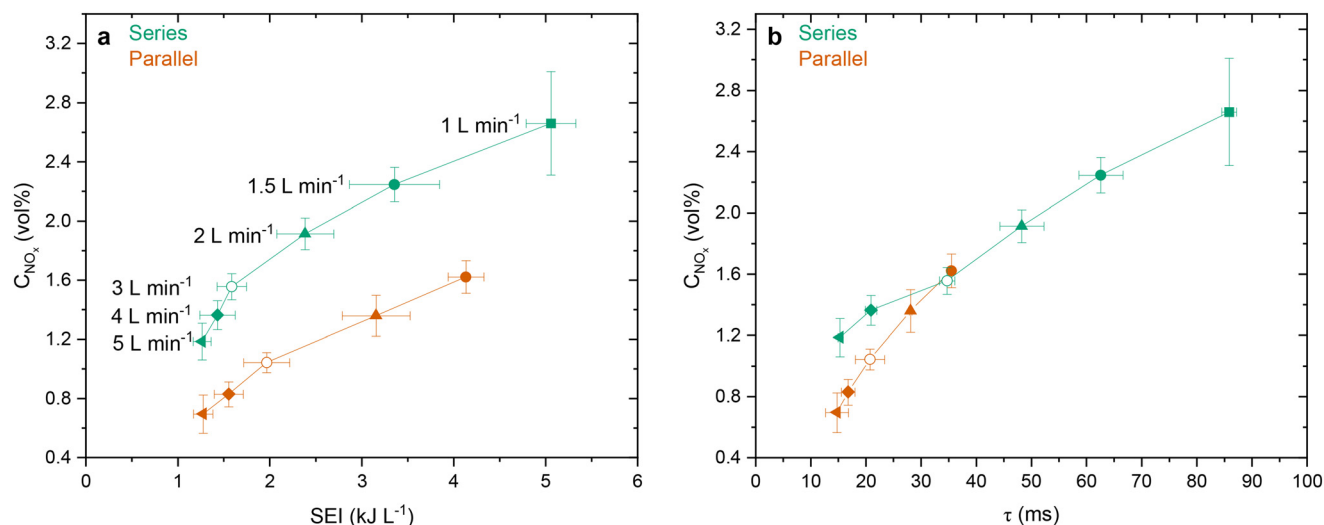This journal is © The Royal Society of Chemistry 2024

Fig. 5 (a) NO_x concentration as function of SEI and (b) effective residence time for the system with series- and parallel-connected reactors.

be observed that the number of current peaks increases at a higher flow rate due to the increasing number of reignitions. As an example, the voltage and current waveforms for both series and parallel topologies at 5 L min^{-1} can be found in Fig. SI.2.2 (a) and (b)†, respectively.

The effect of SEI on the obtained NO_x concentrations in both topologies is shown in Fig. 5(a). The applied SEI ranges were 1.28–4.13 kJ L^{-1} and 1.26–5.06 kJ L^{-1} for the system with parallel- and series-connected reactors, respectively, which resulted in NO_x concentrations between 0.69–1.62 vol%, and 1.19–2.66 vol%. Both cases showed an increase in NO_x concentration with increasing SEI. The increase in NO_x concentration with increasing SEI has been reported in several studies with a single reactor.[35,36] Our results demonstrated that this is also valid for a system featuring two reactors, irrespective of their connection. Additionally, the NO_x concentrations in the series system consistently surpassed those in the parallel system at equivalent SEI levels. Furthermore, the influence of effective residence time on concentration was investigated, results are shown in Fig. 5(b). The NO_x concentration increased with an increase in effective residence time for both series- and parallel-connected reactors. The effective residence time ranges were 14.74–35.49 ms and 15.28–85.87 ms for parallel and series systems, respectively. This indicates the advantage of connecting reactors in series as longer residence time can be achieved, which is beneficial to obtain higher NO_x concentrations. The benefit of enlarging effective residence time to increase the NO_x concentration was also reported by several studies using a single GAR.[23,36] The concentrations of the system with series-connected reactors exceeded the concentrations of the system with parallel-connected reactors in the overlapping range below 20.91 ms, which corresponded to the flow rate of 4 L min^{-1} and above. The observed difference at these flow rates could be a result of the increase in discharge power for the series-connected reactors, as reported in Fig. 2. Moreover, the

discharges in the series system showed a more spark-like behavior with high current peaks comparing to the parallel system, which could also contribute to the elevated concentrations. This is in line with the study of Janda *et al.* who stated that higher rates of atomic N and O could be produced with a transient spark-like discharge, promoting direct atomic recombination to NO and the Zeldovich mechanism.[37]

Fig. 6 shows the NO_2 selectivity as function of SEI for both topologies. An increase in NO_2 selectivity was observed with an increase in SEI for both topologies. A higher SEI could have resulted in an increase in active species, such as atomic oxygen or vibrationally excited oxygen which enhanced the NO oxidation. Maximum selectivities of 46.2 and 37.3% were obtained for series at 5.06 kJ L^{-1} and parallel at 4.13 kJ L^{-1},
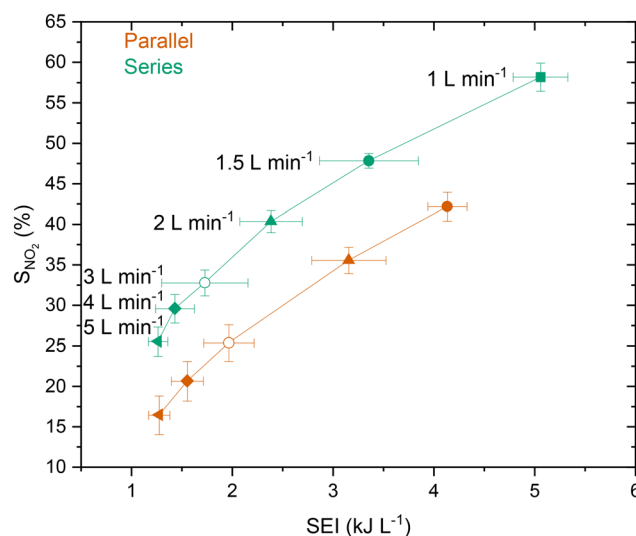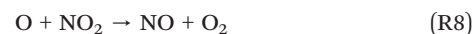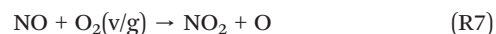

Fig. 6 NO_2 selectivity as function of SEI for the system with series- and parallel-connected reactors.

respectively. The NO$_2$ selectivity obtained in the series-connected reactors consistently surpassed that in parallel-connected reactors at equivalent SEI.

The primary NO$_2$ formation reaction in the GAR at an approximate 80/20 N$_2$ to O$_2$ ratio was reported by Vervloessem *et al.* and was estimated to contribute for 96.1%, which is shown in reaction equation (R6).[38] Furthermore, they estimated the added contribution of the NO reaction with molecular oxygen, whether in a vibrationally excited state or in the ground state (O$_2$ (v/g)) as shown in reaction equation (R7), to be 4.4% only, which was also consistent with the work of Wang *et al.*[39] In addition to the direct electron impact dissociation of NO$_2$, the generated atomic oxygen is also able to dissociate NO$_2$ back to NO and O$_2$ under high temperature conditions, according to reaction equation (R8).[40] Moreover, NO$_2$ dissociation induced by excited N$_2$ could occur as shown in reaction equation (R9). Nevertheless, NO oxidation is kinetically and thermodynamically favorable, at ambient conditions.[41]

$$NO + O(+M) \rightarrow NO_2(+M) \tag{R6}$$

$$NO + O_2(v/g) \rightarrow NO_2 + O \tag{R7}$$

$$O + NO_2 \rightarrow NO + O_2 \tag{R8}$$

$$N_2^* + NO_2 \rightarrow NO + O + N_2 \tag{R9}$$

3.2 Effect of doubling the discharge gap size

Experiments were conducted using a reactor with a doubled gap size (4 mm at the narrowest end), and the results were compared with those obtained from experiments using a single 2 mm reactor. The electrical characteristics differed significantly between these two cases. The current and voltage waveforms in the case of 1 L min^{-1} and 5 L min^{-1} are shown in Fig. 7 as examples.

The increase in flow rate resulted in a decrease in envelope time for both configurations, which was also
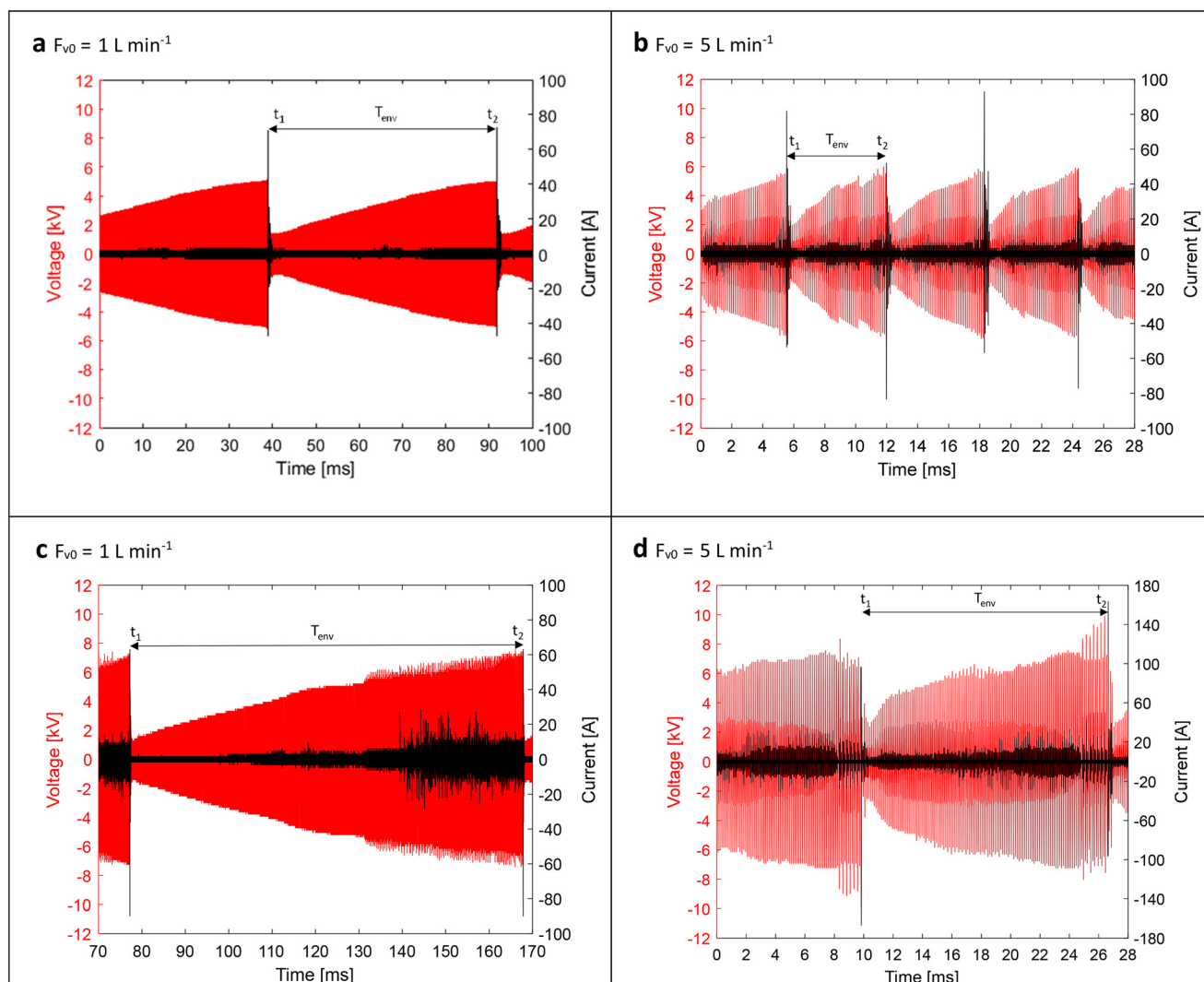

Fig. 7 (a and b) *U–I* plots for 2 mm reactor and (c and d) 4 mm reactor.

5412 | *Catal. Sci. Technol.*, 2024, **14**, 5405–5421

This journal is © The Royal Society of Chemistry 2024

Table 2 Envelope times for different discharge gaps

| F_{v0} (L min^{-1})	$T_{env,2mm}$ (ms)	$T_{env,4mm}$ (ms)
1	54.63 ± 8.62	105.55 ± 19.85
1.5	26.14 ± 5.89	60.71 ± 6.65
2	17.56 ± 7.84	39.63 ± 6.97
3	10.99 ± 5.62	26.87 ± 2.91
4	9.42 ± 4.06	18.92 ± 2.34
5	6.64 ± 2.38	13.97 ± 1.74

observed in the case of series and parallel connected reactors. Table 2 shows the envelope time as a function of flow rate. The envelope time of the 4 mm reactor consistently surpassed that of the 2 mm reactor under the same flow rate, displaying an average increment of 2.2 times. This occurrence could be attributed to the increased discharge gap and subsequent enlargement of the gas channel's cross-section. This led to a reduction in superficial gas velocity under the same flow rate, consequently decreasing the arc propagation velocity. As a result, the arc was sustained for a longer period of time, before arc extinguishment occurred. Furthermore, different maximum voltages were observed for the 2 and 4 mm reactors at equal flow rates as shown in Fig. 7. The maximum voltages are related to the size of the gap at which the maximum arc height was reached. The gap at maximum height in the case of 4 mm reactors is always larger than for the 2 mm reactor, hence a higher maximum voltage is required for gas breakdown. The absence of current-peaks apart from the tens of ampere sparks in Fig. 7(a), indicate a glow-like discharge within the 2 mm reactor, whereas Fig. 7(c) could be more compared to a glow to spark-like transitional discharge for the 4 mm reactor.

The discharge powers were calculated with eqn (4) and shown in Fig. 8. It is evident that the discharge power in the 4 mm reactor is higher than that of the 2 mm reactor. This outcome aligns with the observation of higher voltage and

current. Nevertheless, the discharge power remains less than twice the one exhibited in the 2 mm reactor. A similar U-shaped trend of power variation with flow rate was observed in both cases with a minimum value obtained at 2 L min^{-1}.

Differences in arc height were observed for both reactors with different discharge gaps. Fig. 9(a) shows two photographs for both discharge gaps at a flow rate of 1 L min^{-1}. The figure shows that the arc height in the 4 mm reactor case exceeded the arc height of the 2 mm reactor; besides, the arc in case of 4 mm reactor reached the top of the electrodes, which therefore limited potential further propagation and an increase in plasma volume. Furthermore, the figure shows that the arc was brighter at the top of the 4 mm electrodes. The plasma volumes were calculated, and the results are shown in Fig. 9(b). The plasma volume in the case of 2 mm reactor has no significant change until 3 L min^{-1}, whereafter it gradually increased with an increase in flow rate. Furthermore, the plasma volume in the case of 4 mm reactor decreased at 5 L min^{-1}. The effective residence time in both cases, calculated based on the plasma volume and corresponding flow rate, along with its difference, is shown in Fig. 9(c). An increase in flow rate resulted in a decrease in effective residence time and absolute difference for both configurations. Maximum effective residence times of 50.4 and 91.1 ms were determined at 1 L min^{-1} for 2 and 4 mm reactors, respectively. Minimum residence times of 13.7 and 15.3 ms were obtained at 5 L min^{-1}, which corresponded to a difference of only 1.6 ms.

The obtained NO$_x$ concentration in different cases as a function of SEI is shown in Fig. 10(a). An increase in SEI resulted in an increase in NO$_x$ concentration in both cases. The applied SEI ranges were 0.74–3.60 kJ L^{-1} for the 2 mm reactor and 1.12–5.78 kJ L^{-1} for the 4 mm reactor. Maximum concentrations of 1.06 and 1.45 vol% for 2 and 4 mm reactors were obtained, respectively. The increase of NO$_x$ concentration in case of the 2 mm reactor decreased after a SEI of 1.27 kJ L^{-1}. A possible explanation for this reduction could be the increase of nitric oxide dissociation reactions in the relatively small plasma volume, compared to the 4 mm reactor. An increase in SEI could result in an intensification of atomic oxygen and atomic nitrogen, which could reduce NO as shown in reaction equation (R10) and (R11).[42] Besides, NO can also be reduced with activated N$_2$, as shown in (R12). Nevertheless, the occurrence of these species is also essential for NO$_x$ synthesis. Therefore it is essential to maintain an optimal balance between NO$_x$ synthesis and dissociation. Moreover, the reduction in the increase of reaction product with increasing SEI was also observed by Ivanov et al.; however, for CO$_2$ splitting in a similar 2D-GAR.[43] The authors also assigned occurring back-reactions as possible reason and proposed quenching as a solution to prevent the formation of the occurring concentration-plateau.
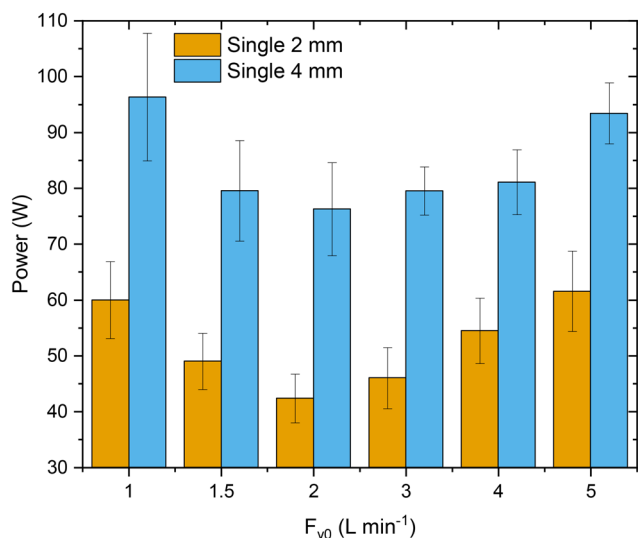
Fig. 8 Discharge powers for both 2 and 4 mm reactor configurations.
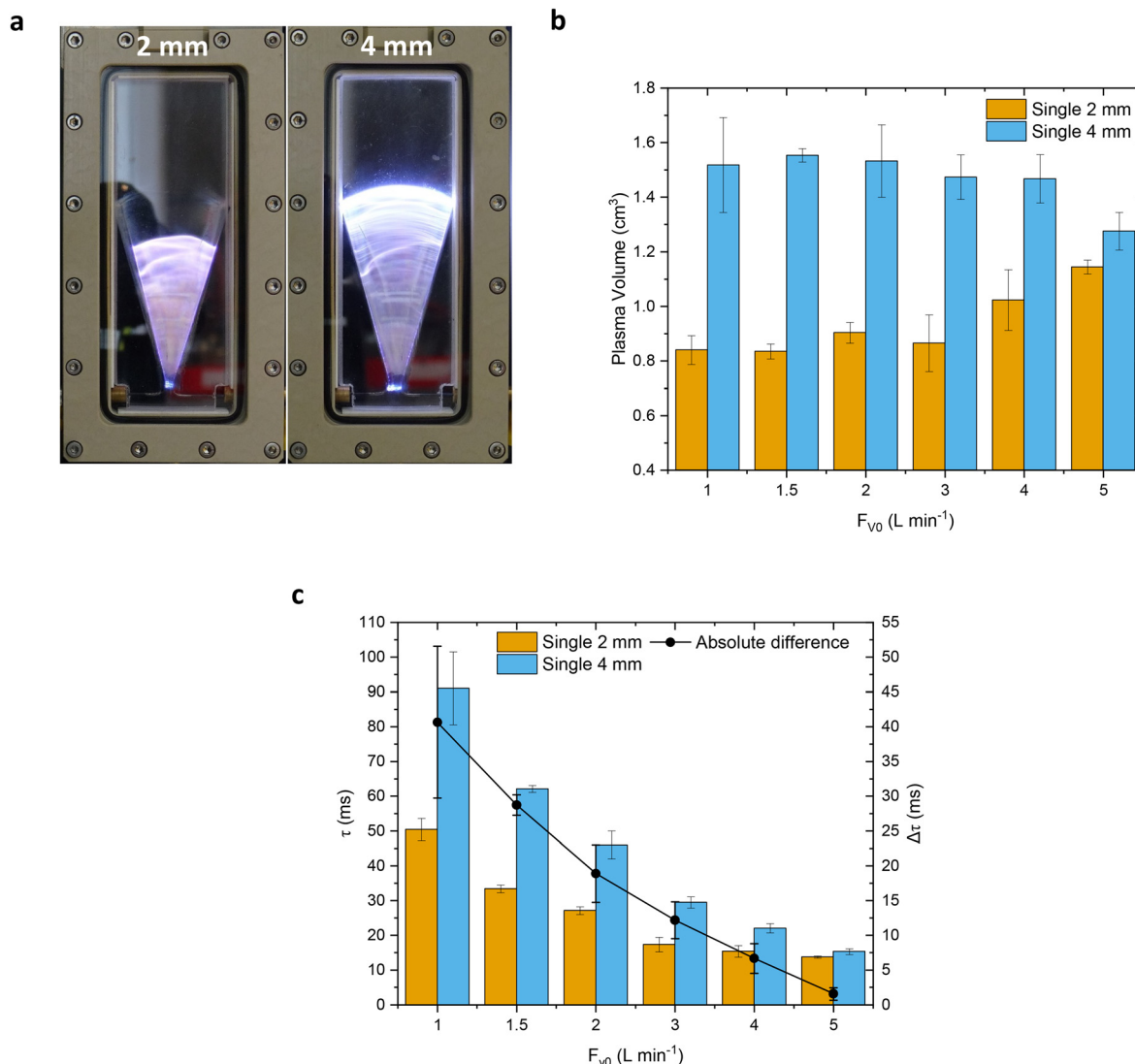
$$NO + N \rightarrow O + N_2 \qquad (R10)$$

Fig. 9 (a) Arc propagation for the 2 mm and 4 mm discharge gap at 1 L min^{-1}. (b) Plasma volume and (c) effective residence time for the 2 and 4 mm discharge gap as function of feed flow rate.

$$NO + O \rightarrow N + O_2 \qquad (R11)$$

$$NO + N_2^* \rightarrow N_2 + N + O \qquad (R12)$$

In Fig. 10(b), an approximately linear increase in NO_x concentrations was observed when increasing the effective residence time for both the 2 and 4 mm discharge gap. Both Fig. 10(a) and (b) emphasize the importance of effective residence time, on par with SEI, in influencing NO_x concentrations. The 4 mm reactor can be operated at longer effective residence time, which is beneficial to increase the NO_x concentration. At low effective residence times around the region of 10 ms, a rapid increase in NO_x concentration was observed even with a minor increase in effective residence time. Limited improvements can be made in increasing the effective

residence time for the current 4 mm discharge gap reactor, since the arc has already reached the top as shown in Fig. 9(a). Therefore, further reactor development is necessary. It should be noted that the concentration is not solely influenced by the residence time, therefore the other factors such as power could contribute to this change.

The NO_2 selectivity was investigated for both discharge gaps as function of SEI and shown in Fig. 11. An increase in NO_2 selectivity was observed with an increase in SEI for both configurations. Maximum selectivities of 41.6 and 43.7% were obtained at a flow rate of 1 L min^{-1}, for 2 and 4 mm reactors, respectively. Although the discharge mode and discharge power were different for both configurations, the maximum observed selectivity difference was only 8.9% at a SEI of 1.27 kJ L^{-1}.
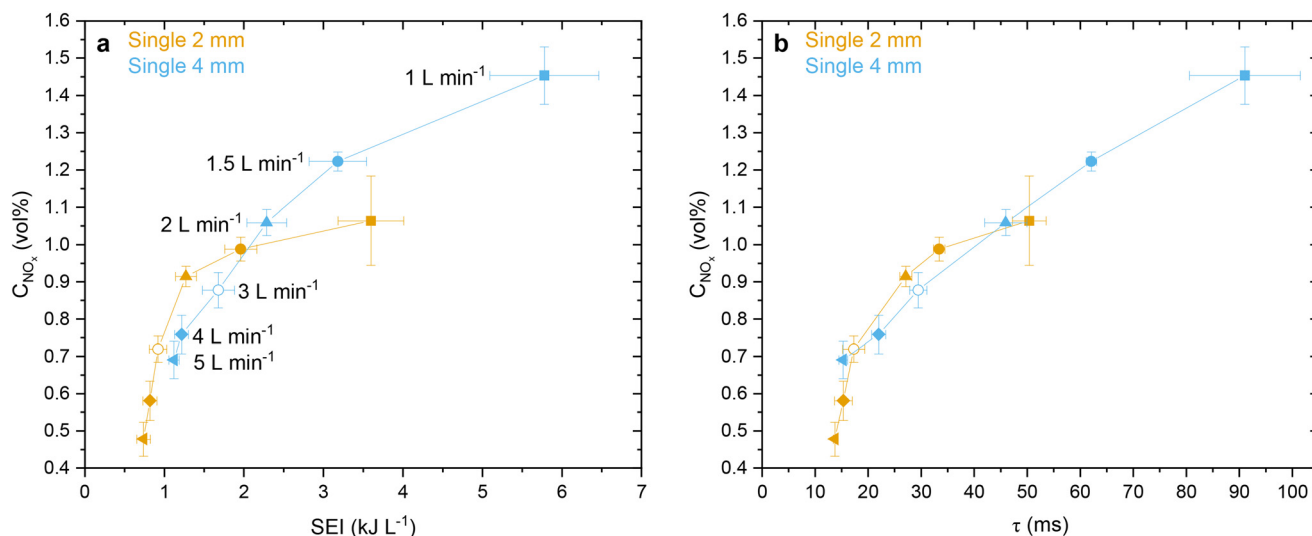
5414 | *Catal. Sci. Technol.*, 2024, **14**, 5405–5421

This journal is © The Royal Society of Chemistry 2024

Fig. 10 (a) NO$_x$ concentration as function of SEI and (b) effective residence time for the 2 and 4 mm discharge gap.

3.3 Overall considerations on implementing the different configurations

The generalized reaction equation (R13) describes the possible reversible formation of NO$_x$ in air plasma. Subsequently, the synthesized NO can oxidize to NO$_2$ and NO$_2$ can dimerize to N$_2$O$_4$ as previously shown in reaction equations (R5) and (R4), respectively. The total molar flow rate of reactive nitrogen F_{N_r} (mmol h^{-1}) can be calculated by eqn (7), where F_{T0} (mmol h^{-1}) represents the initial number of moles in the feed and y_i is the measured volume fraction of every form of reactive nitrogen. The derivation of eqn (7) can be found in section SI.3 of the ESI,† along with the quantification of the initial molar flow rate as function of volumetric feed flow rate.

$$N_2 + XO_2 \rightleftharpoons 2NO_x \qquad (R13)$$

$$F_{N_r}\left(\text{mmol h}^{-1}\right) = \frac{F_{T0}\left(\text{mmol h}^{-1}\right)\cdot\left(y_{NO} + y_{NO_2} + 2y_{N_2O_4}\right)}{1 + 0.5y_{NO_2} + 2y_{N_2O_4}} \qquad (7)$$

Fig. 12(a) was constructed to generate a direct overview of the overall efficiency of the four discussed configurations, which shows the energy consumption as function of the absolute amount of NO$_x$ produced. The figure indicates an increase in process efficiency with increased flow rate, since more NO$_x$ production and a decrease in EC was observed. However, it is a fact that the concentration of NO$_x$ decreased with the increase of flow rate in all tested cases, due to the decrease in effective residence time as previously shown in Fig. 5(b) and 10(b). Considering the practical application, one or more follow-up processes are needed. For example, reaction equation (R3) is required to produce a nitrate solution. In this case, certain NO$_2$ concentrations needed to be maintained to prevent mass transfer limitations of NO$_2$ to the liquid interface.[44]

More importantly, Fig. 12(a) shows that the reactors connected in series outperformed all the other configurations, since an EC range of 2.29–2.42 MJ mol^{-1} was obtained with corresponding NO$_x$ productions of 124.6–158.3 mmol h^{-1}. The increase in spark-like discharge behavior without drastically increasing the discharge power could be one of the prevailing factors. Furthermore, it is important to note that while more NO$_x$ production can be achieved in series-connected reactors, this enhancement effect is significantly influenced by the number of reactors connected. Our work focuses on the fundamental connection with only two reactors, but the complexity of the discharge behavior and power dissipation will increase with more reactors. Moreover, as the residence time of the reactants increases when passing through more reactors, both the formation and
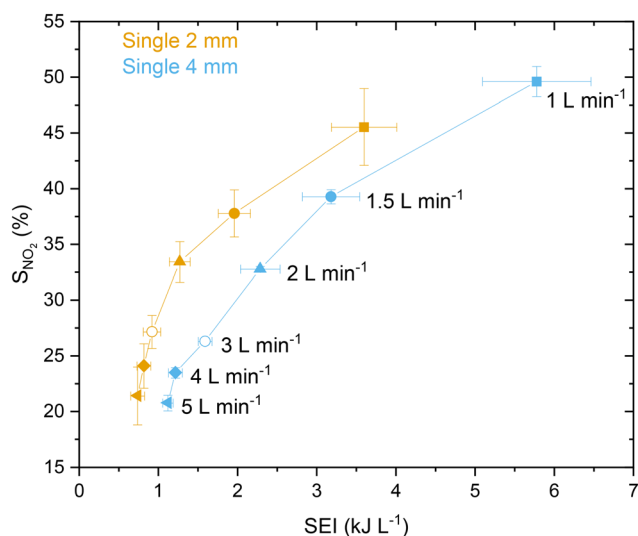

Fig. 11 NO$_2$ selectivity as function of SEI for the 2 mm reactor and 4 mm reactor.

This journal is © The Royal Society of Chemistry 2024

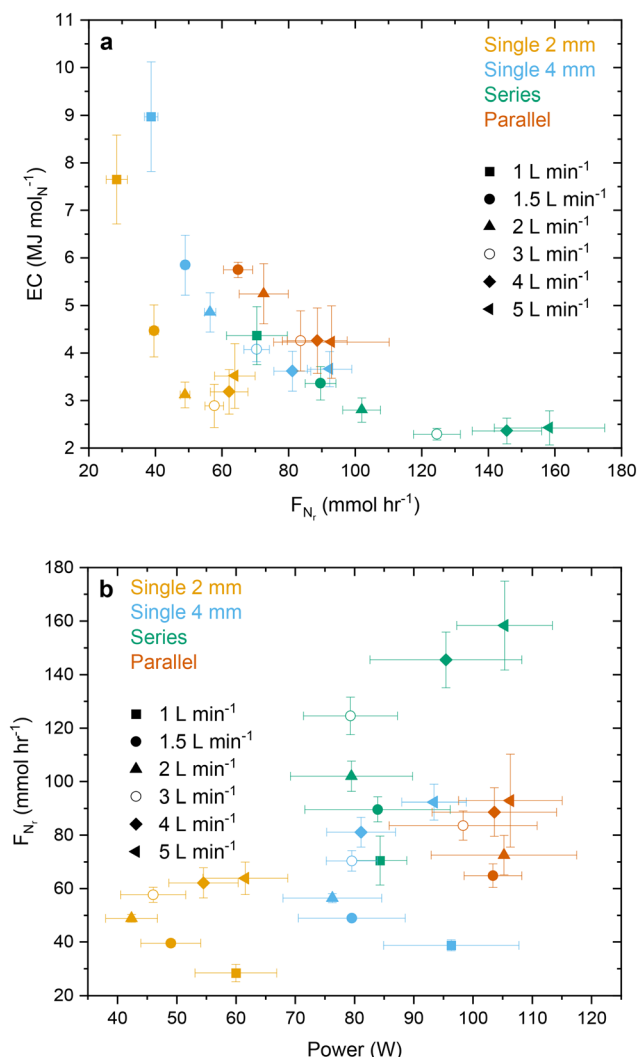*Catal. Sci. Technol.*, 2024, **14**, 5405–5421 | **5415**

Fig. 12 (a) The energy consumption as function of absolute produced amount of NO_x and (b) the absolute produced amount of NO_x as function of power for all four considered cases.

dissociation reactions will be enhanced. The dissociation reactions may become more significant as higher concentrations of NO_x are reached. Therefore, it is important to find an optimal number of reactors in order to achieve a balance between the formation and dissociation reactions. Besides, another comparison was made, based between a

system with series-connected reactors and a system with two identical reactors operated separately, with the same discharge gap of 2 mm. The absolute productions and ECs of both systems are shown in Table 3. This table shows that the performance of the reactors connected in series outperformed the case of two identical reactors operated separately, as shown in Table 3.

An overview of the absolute amounts of NO_x produced as a function of power for all tested cases is shown in Fig. 12(b). It should be noted that this study focuses on the energy consumption of the reactors instead of the overall electrical system. This aligns with most reported studies in this field, ensuring direct comparability with other works. Due to variations in the electrical systems used by different researchers, particularly the power supply, the energy consumption of the entire system cannot be directly compared and is therefore often not reported. However, the overall energy consumption is crucial to the plasma process. When multiple GARs are connected in the system, the load profile changes with the number of reactors and their operation. Consequently, the overall power consumption and its distribution in the circuit vary. This introduces complexity to the analysis and optimization of the overall system, but it is an issue that requires attention when considering scaling up the reactor *via* the numbering up approach.

All cases except the system with parallel-connected reactors show a C-shaped profile. This shape is presumably the result of similarities in arc dynamics, that merit further investigation in future work. A key factor that needs mentioning is that a different power can be delivered by using different strategies. In general, the power order follows: single 2 mm reactor < single 4 mm reactor ≈ series connected reactors < parallel connected reactors. Moreover, the figure indicates that the single 4 mm reactor outperformed the parallel connected reactor when applying elevated flow rates, *i.e.* 4 and 5 L min^{-1}. Similar productions could be obtained at lower ECs. This is probably due to the increased effective residence times of CDA in the case of 4 mm reactor, while consuming less power than the parallel system. Besides, only one GAR is required in this case, which reduces the capital expenditure. Finally, the electrical circuit is easier to control with a single GAR as discussed in section 3.1, which also simplifies potential process optimization.

Table 3 Absolute produced amounts of reactive nitrogen and energy consumptions for the system of series-connected reactors and the system of two identical single 2 mm reactors

F_{v0} (L min^{-1})	$F_{N,\ series}$ (mmol h^{-1})	$F_{N,\ 2\times single\ 2mm}$ (mmol h^{-1})	EC, $_{series}$ (MJ mol^{-1})	EC, $_{2\times single\ 2mm}$ (MJ mol^{-1})
1	70.49 ± 9.15	56.81 ± 6.37	4.37 ± 0.61	7.65 ± 0.94
1.5	89.60 ± 4.61	79.15 ± 2.56	3.36 ± 0.35	4.47 ± 0.55
2	101.98 ± 5.67	97.72 ± 2.91	2.80 ± 0.26	3.12 ± 0.27
3	124.56 ± 7.03	115.36 ± 5.60	2.29 ± 0.12	2.89 ± 0.45
4	145.56 ± 10.43	124.27 ± 11.30	2.36 ± 0.27	3.18 ± 0.47
5	158.34 ± 16.60	127.72 ± 12.15	2.42 ± 0.36	3.52 ± 0.68

5416 | *Catal. Sci. Technol.*, 2024, **14**, 5405–5421

This journal is © The Royal Society of Chemistry 2024

3.4 Plasma-catalytic considerations and post-plasma NO oxidation

The use of catalysts in combination with plasma could improve the energy efficiency and selectivity of the products, and has gained significant interest in the field of gas conversion. Plasma-catalytic nitrogen fixation has also been the subject of considerable attention in the scientific community over the past decade.[45] However, the majority of research in this field is concentrated on the synthesis of NH_3 rather then NO_x.[46,47] Nonetheless, the works of Patil *et al.* and Zhang *et al.* employed a plasma-catalytic DBD reactor containing a metal oxide for the synthesis of NO_x.[48,49] Although increased NO_x concentrations were achieved, they attributed the enhancement effect to an increase of microdischarges and surface area, as well as an enhancement of the electric-field near the catalytic surface and sharp edges, while clear evidence of plasma-catalytic surface reactions was not provided. In fact, catalytic materials that effectively utilize the reactive species generated by plasma for surface reactions contributing to the formation of NO_x have been rarely reported so far. The synthesis of NO_x in plasma reactors is predominantly driven by gas-phase reactions induced by plasma. This raises the question of whether the use of catalysts is necessary in such cases.

Additionally, the method of introducing catalysts into a plasma reactor is a critical factor to consider. The so-called 'in-plasma' catalysts (IPC), which directly packs the catalysts in the discharge zone, can be easily implemented in DBD reactors. However, the performance of DBD reactors for NO_x synthesis is not favorable. In contrast, warm plasma reactors such as gliding arc and microwave reactors, which perform better in NO_x synthesis, often reach high temperatures around several thousand Kelvin, which could directly alter the catalyst structure and intrinsic properties.[50] Therefore, post-plasma catalysts (PPC) are preferred. Nevertheless, maintaining sufficient interaction between the short-lived plasma species and catalysts in this case is challenging. In summary, the benefit of using a plasma-catalytic system for NO_x synthesis with a GAR is not clear due to the limited evidence of existing plasma-catalytic synergy, the increased complexity of catalyst implementation, and the rising cost of the overall process.

Tuning selectivity is one possible reason to implement catalysts in the post-plasma zone. In our case, achieving high NO_2 selectivity is important as it directly impacts reactions like equation (R3), which are crucial for applications such as nitric acid or fertilizer production. However, the NO oxidation as shown in equation (R5) is exergonic and exothermic, hence the reaction will occur spontaneously and is favored at low temperatures as long as there is oxygen or NO present in the reaction zone.[51] This means that it could easily occur in transport or storage. In our case, oxidation occurs even in the tubing from the reactor outlet to the FTIR cell. To quantify the influence of post-plasma oxidation, analysis was made based on the time corresponding to gas passing through the tubing from the outlet of the plasma reactor to the FTIR cell. This time ranges from 1.6 to 7.8 s corresponding to the flow rate of 5 to 1 L min^{-1}, respectively, which was calculated using eqn (8). The NO concentration at the GAR's exit, denoted as $[NO]_{GAR}$, was determined based on the measured NO concentration in the FTIR, the reaction rate constant (k (L^2 mol^{-1} s^{-1})) defined by Tsukahara *et al.*,[41] the oxygen concentration ($[O_2]$), and the total oxidation time in the post-plasma volume ($\tau_{oxidation}$), as shown in eqn (9). Due to the high oxygen concentration compared to the NO concentration, it was assumed that the oxygen concentration remained constant, and that the reaction followed pseudo-second-order kinetics. The oxygen volume fraction in the feed was 21 vol%, and its concentration was calculated using the ideal gas law, considering the FTIR inlet temperature and pressure. Rapid heat transfer with the metallic wall tubing and ambient air kept the post-plasma temperature isothermal at 20 °C. Potential pressure drop was not included in the calculation. The measured concentrations are presented in parentheses (mol L^{-1}). The derivation of eqn (9) can be found in section SI.4. of the ESI.† Furthermore, the conversion of NO oxidation was calculated *via* eqn (10).

$$\tau_{oxidation}(s) = \frac{V(L) \cdot 60(s\ min^{-1})}{F_{v0}(L\ min^{-1})} \quad (8)$$

$$[NO]_{GAR} = \frac{[NO]}{(1 - 2k[O_2][NO]\tau_{oxidation}(s))} \quad (9)$$

$$X_{NO}(\%) = \frac{[NO]_{GAR} - [NO]}{[NO]_{GAR}} \cdot 100\% \quad (10)$$

Fig. 13(a) shows that NO_2 selectivity increases obviously with total oxidation time across all four reactor configurations. The reactors in series achieved slightly higher NO_2 selectivities, with a maximum of 46.2%, although the difference compared to single 2 mm and 4 mm configurations was only 4.6% and 2.5%, respectively.

Taking the case with a feed flow rate of 1 L min^{-1} as an example, the theoretical NO conversion as a function of time is shown in Fig. 13(b). A steep increase in NO conversion is observed initially, followed by a mild increase towards a plateau due to the rapid drop in NO concentration. The time to achieve 95% NO conversion varied among different configurations, with the shortest time for reactors in series (112.8 s) and the longest for the single 2 mm configuration (282.9 s). This is mainly due to the difference in the initial concentration of NO, which is determined by the performance of the plasma reactors. Furthermore, it can be deduced that achieving higher conversions requires relatively long oxidation times. However, enabling the required oxidation time can be simply achieved by increasing the post-plasma volume or adding a storage unit. These are more viable options than deploying a catalyst, which would simultaneously increase the cost and complexity of the overall process.
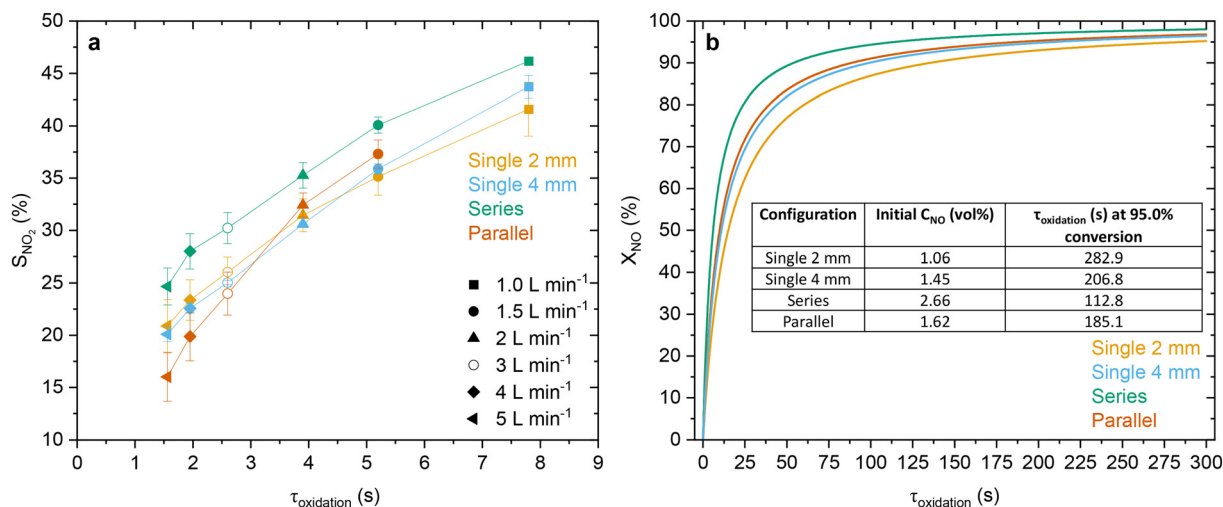
This journal is © The Royal Society of Chemistry 2024

Catal. Sci. Technol., 2024, **14**, 5405–5421 | **5417**

Fig. 13 (a) The NO_2 selectivity as a function of total oxidation time for all four considered cases. (b) The theoretical NO conversion as a function of time.

Table 4 Overview of recently published works in the plasma based NO_x synthesis. Adapted and complemented from the work of Li *et al.* 2023, with permission of ACS Sustainable Chem. Eng. Under license CC-BY 4.0 (ref. 25)

Plasma/reactor	Max C_{NO_x} (vol%)	EC (MJ mol_N^{-1})	F_{v0} (L min^{-1})	N_2/O_2 ratio	P_{abs} (atm)
Rotating GAR[52]	5.5	2.5	2.0	50:50	1
Plasma soft jet[27]	0.02	0.42	1.5	78:21	1
Rotating GAR (nozzle)[22]	5.9	2.1	2.0	50:50	1
Rotating GAR[36]	0.28	0.67	170.0	78:21	1
DC glow discharge[53]	0.7	2.8	10.0	78:21	1
Propeller arc[54]	0.45	4.2	0.3	20:10	1
Plasmatron[38]	1.5	3.6	10.0	70:30	1.23
MW plasma[18]	3.8	2.0	0.77	50:50	1
2D-GAR d_{gap} 6.20 mm[25]	1.43	6.95	0.5	78:21	1
Rotating GAR (elevated P)[23]	2.4	1.8	12.0	50:50	4
Spark discharge reactor[55]	3.0	4.4	1.0	50:50	1
Dielectric-boosted GAR with TiO_2 [56]	~0.26	—	2.4	70:30	1
Single 2D-GAR d_{gap} 2.0 mm	1.06	7.65	1.0	78:21	1.1
	0.91	2.89	3.0		1.2
Single 2D-GAR d_{gap} 4.0 mm	1.45	8.97	1.0	78:21	1.1
	0.76	3.62	4.0		1.2
Parallel 2D-GARs	1.62	5.75	1.5	78:21	1.1
	0.69	4.23	5.0		1.3
Series 2D-GARs	2.66	4.37	1.0	78:21	1.1
	1.56	2.29	3.0		1.2

4. Conclusions

This study examined two strategies to enhance the plasma-based NO_x production using GARs. The first strategy investigated two systems, one with a configuration of two series-connected reactors and a second configuration with two parallel-connected reactors. The second strategy investigated the effect of increasing the discharge gap of a single GAR. The results are summarized in Table 4, along with data from recently published works for comparison. The maximum concentration of NO_x and energy consumption achieved in the four tested cases are within the ranges reported in the literature. Optimization of operation and reactor design was not performed, as this work focuses on the connection configurations. Nevertheless, a 20.9% improvement in EC was achieved by applying two series-connected reactors compared to the single 2 mm reactor.

As reported by Rouwenhorst *et al.*, the EC of the process should be equal to or below 1.5 MJ mol_N^{-1} to become a highly competitive alternative to the Haber–Bosch process combined with the Ostwald process.[57] In this work, the minimum EC obtained was 2.29 MJ mol_N^{-1} for reactors connected in series and 4.23 MJ mol_N^{-1} for reactors connected in parallel. These values are higher than the target objective, indicating further improvement is required. Further optimization can be done to the reactor design and operating parameters, which was not explored in our study. Nevertheless, the enhancement achieved in multi-reactor

5418 | *Catal. Sci. Technol.*, 2024, **14**, 5405–5421

This journal is © The Royal Society of Chemistry 2024

operation demonstrated potential for further improvement of overall process performance towards the objective of 1.5 MJ mol_N^{-1}.

Additionally, increased NO_x concentrations were obtained by multi-reactor operation as well as by sizing up the reactor from 2 mm to 4 mm. However, using a larger reactor did not show advantages in EC under the tested conditions. In principle, scaling up the reactors could cause stability issues due to the increased breakdown voltage required. Similar issues exist when operating multiple reactors connected electrically in series, but these can be better controlled with a modular system comprising multiple reactors, which have moderate minimum discharge gaps. Nevertheless, the results also showed that a numbered-up system introduces additional complexity and, consequently, instability to the overall system due to a change in load and power profile. Regarding cost, the numbering up strategy, which implements more reactors, generally leads to a higher capital expenditure (CAPEX). However, this is expected to decrease due to a learning factor during technology development. On the other hand, operational expenditure (OPEX) is directly related to the EC, which would favor reactors connected in series as demonstrated in this work.

All four tested cases demonstrated an increase in NO_x concentration when the SEI and effective residence time were increased. This result indicated that adjusting these two process parameters is still effective in improving the process, even when two reactors are used. Additionally, the concentration of NO_x was consistently higher for the system with series-connected reactors compared to the system with parallel-connected reactors. This effect was mainly due to the longer effective residence times and the resulting increase in spark-like discharge behavior caused by differences in superficial gas velocity. Moreover, increasing the discharge gap from 2 to 4 mm reactors in a single GAR resulted in extended effective residence times and SEIs, as well as an increase in the number of current peaks. This enhancement reflects similar benefits to the series system. Furthermore, further discussion was provided regarding the implementation and utilization of a catalyst in the current system. Additionally, the results demonstrate that the NO_2 selectivity can be readily enhanced by prolonging the post-plasma oxidation time, as opposed to adjusting the plasma parameters or incorporating post-plasma oxidation units. Implementing these strategies and optimization of process conditions could facilitate the transition of plasma-based NO_x fixation towards industrialization.

Data availability

The data supporting this article have been included as part of the ESI.†

Conflicts of interest

There are no conflicts to declare.

Acknowledgements

References

1 D. Fowler, M. Coyle, U. Skiba, M. A. Sutton, J. N. Cape and S. Reis, *et al.*, The Global Nitrogen Cycle in the Twenty-First Century, *Philos. Trans. R. Soc., B*, 2013, **368**(1621), 20130164, DOI: **10.1098/rstb.2013.0164**.

2 S. Fields, Global Nitrogen: Cycling out of Control, *Environ. Health Perspect.*, 2004, **112**(10), 556–563, DOI: **10.1289/ehp.112-a556**.

3 V. Smil, Nitrogen in Crop Production: An Account of Global Flows, *Global Biogeochem. Cycles*, 1999, **13**(2), 647–662.

4 Y. Tanabe and Y. Nishibayashi, Developing More Sustainable Processes for Ammonia Synthesis, *Coord. Chem. Rev.*, 2013, **257**(17–18), 2551–2564, DOI: **10.1016/j.ccr.2013.02.010**.

5 H. Liu, Ammonia Synthesis Catalyst 100 Years: Practice, Enlightenment and Challenge, *Chin. J. Catal.*, 2014, **35**(10), 1619–1640, DOI: **10.1016/S1872-2067(14)60118-2**.

6 I. Rafiqul, C. Weber, B. Lehmann and A. Voss, Energy Efficiency Improvements in Ammonia Production - Perspectives and Uncertainties, *Energy*, 2005, **30**(13), 2487–2504, DOI: **10.1016/j.energy.2004.12.004**.

7 FAO, *World Food and Agriculture - Statistical Yearbook 2021*, Rome, 2021.

8 FAO, IFAD, UNICEF, WFP and WHO, *The State of Food Security and Nutrition in the World 2022. Repurposing Food and Agricultural Policies to Make Healthy Diets More Affordable*, Rome, 2022, DOI: **10.1016/S2213-8587(22)00220-0**.

9 U.S. Census Bureau. International Database. https://www.census.gov/data-tools/demo/idb/#/country?COUNTRY_YEAR=2050&COUNTRY_YR_ANIM=2050 (accessed 2022-10-14).

10 N. Cherkasov, A. O. Ibhadon and P. Fitzpatrick, A Review of the Existing and Alternative Methods for Greener Nitrogen Fixation, *Chem. Eng. Process.*, 2015, **90**, 24–33, DOI: **10.1016/j.cep.2015.02.004**.

11 A. Fridman, *Plasma Chemistry*, 2008, pp. 1–978, DOI: **10.1017/CBO9780511546075**.

12 S. Li, J. A. Medrano, V. Hessel and F. Gallucci, Recent Progress of Plasma-Assisted Nitrogen Fixation Research: A Review, *Processes*, 2018, **6**, 248, DOI: **10.3390/pr6120248**.

13 A. Bogaerts and E. C. Neyts, Plasma Technology: An Emerging Technology for Energy Storage, *ACS Energy Lett.*, 2018, **3**(4), 1013–1027, DOI: **10.1021/acsenergylett.8b00184**.

14 T. A. B. J. van Raak, S. Li and F. Gallucci, Prevailing Surface Reactions in the Plasma-Catalytic Ammonia Synthesis with Ru/CeO2 and Ru/Ti-CeO2, *Chem. Eng. J.*, 2023, **455**, 1–10, DOI: **10.1016/j.cej.2022.140691**.

15 S. Li, T. van Raak and F. Gallucci, Investigating the Operation Parameters for Ammonia Synthesis in Dielectric Barrier Discharge Reactors, *J. Phys. D: Appl. Phys.*, 2020, **53**(1), 014008, DOI: **10.1088/1361-6463/ab4b37**.

This journal is © The Royal Society of Chemistry 2024

Catal. Sci. Technol., 2024, **14**, 5405–5421 | **5419**

16 Y. Gorbanev, Y. Engelmann, K. van't Veer, E. Vlasov, C. Ndayirinde, Y. Yi, S. Bals and A. Bogaerts, Al$_2$O$_3$-Supported Transition Metals for Plasma-Catalytic NH$_3$ Synthesis in a DBD Plasma: Metal Activity and Insights into Mechanisms, *Catalysts*, 2021, **11**, 1230, DOI: **10.3390/catal11101230**.

17 P. Peng, Y. Li, Y. Cheng, S. Deng, P. Chen and R. Ruan, Atmospheric Pressure Ammonia Synthesis Using Non-Thermal Plasma Assisted Catalysis, *Plasma Chem. Plasma Process.*, 2016, **36**(5), 1201–1210, DOI: **10.1007/s11090-016-9713-6.**

18 S. Kelly and A. Bogaerts, Nitrogen Fixation in an Electrode-Free Microwave Plasma, *Joule*, 2021, **5**(11), 3006–3030, DOI: **10.1016/j.joule.2021.09.009.**

19 J. Lee, H. Sun, S. K. Im and M. Soo Bak, Formation of Nitrogen Oxides from Atmospheric Electrodeless Microwave Plasmas in Nitrogen-Oxygen Mixtures, *J. Appl. Phys.*, 2017, **122**(8), DOI: **10.1063/1.4996790.**

20 X. Pei, D. Gidon and D. B. Graves, Specific Energy Cost for Nitrogen Fixation as NOx using DC Glow Discharge in Air, *J. Phys. D: Appl. Phys.*, 2020, **53**(4), DOI: **10.1088/1361-6463/ab5095.**

21 Z. Y. Li, L. L. Nie, D. W. Liu and X. P. Lu, An Atmospheric Pressure Glow Discharge in Air Stabilized by a Magnetic Field and Its Application on Nitrogen Fixation, *Plasma Processes Polym.*, 2022, **19**(12), DOI: **10.1002/ppap.202200071**.

22 S. Van Alphen, H. Ahmadi Eshtehardi, C. O'Modhrain, J. Bogaerts, H. Van Poyer and J. Creel, *et al.*, Effusion Nozzle for Energy-Efficient NOx Production in a Rotating Gliding Arc Plasma Reactor, *Chem. Eng. J.*, 2022, **443**, 136529, DOI: **10.1016/j.cej.2022.136529.**

23 I. Tsonev, C. O'Modhrain, A. Bogaerts and Y. Gorbanev, Nitrogen Fixation by an Arc Plasma at Elevated Pressure to Increase the Energy Efficiency and Production Rate of NO X, *ACS Sustainable Chem. Eng.*, 2023, 2–11, DOI: **10.1021/acssuschemeng.2c06357.**

24 F. Jardali, S. Van Alphen, J. Creel, H. Ahmadi Eshtehardi, M. Axelsson and R. Ingels, *et al.*, NOx Production in a Rotating Gliding Arc Plasma: Potential Avenue for Sustainable Nitrogen Fixation, *Green Chem.*, 2021, **23**(4), 1748–1757, DOI: **10.1039/d0gc03521a.**

25 S. Li, T. van Raak, R. Kriek, G. De Felice and F. Gallucci, Gliding Arc Reactor under AC Pulsed Mode Operation: Spatial Performance Profile for NO$_x$ Synthesis, *ACS Sustainable Chem. Eng.*, 2023, **11**(34), 12821–12832, DOI: **10.1021/acssuschemeng.3c03832.**

26 S. Van Alphen, V. Vermeiren, T. Butterworth, D. C. M. Van Den Bekerom, G. J. Van Rooij and A. Bogaerts, Power Pulsing to Maximize Vibrational Excitation Efficiency in N$_2$ Microwave Plasma: A Combined Experimental and Computational Study, *J. Phys. Chem. C*, 2020, **124**(3), 1765–1779, DOI: **10.1021/acs.jpcc.9b06053.**

27 E. Vervloessem, Y. Gorbanev, A. Nikiforov, N. De Geyter and A. Bogaerts, Sustainable NO: Xproduction from Air in Pulsed Plasma: Elucidating the Chemistry behind the Low Energy Consumption, *Green Chem.*, 2022, **24**(2), 916–929, DOI: **10.1039/d1gc02762j.**

28 I. Adamovich, S. Agarwal, E. Ahedo, L. L. Alves, S. Baalrud and N. Babaeva, *et al.*, The 2022 Plasma Roadmap: Low Temperature Plasma Science and Technology, *J. Phys. D: Appl. Phys.*, 2022, **55**(37), DOI: **10.1088/1361-6463/ac5e1c**.

29 H. K. Roscoe and A. K. Hind, The Equilibrium Constant of NO2 with N2O4 and the Temperature Dependence of the Visible Spectrum of NO2: A Critical Review and the Implications for Measurements of NO2 in the Polar Stratosphere, *J. Atmos. Chem.*, 1993, **16**(3), 257–276, DOI: **10.1007/BF00696899**.

30 B. Hüpen and E. Y. Kenig, Rigorous Modelling of NOx Absorption in Tray and Packed Columns, *Chem. Eng. Sci.*, 2005, **60**(22), 6462–6471, DOI: **10.1016/j.ces.2005.04.060**.

31 J. Zhu, Z. Sun, Z. Li, A. Ehn, M. Aldén and M. Salewski, *et al.*, Dynamics, OH Distributions and UV Emission of a Gliding Arc at Various Flow-Rates Investigated by Optical Measurements, *J. Phys. D: Appl. Phys.*, 2014, **47**(29), DOI: **10.1088/0022-3727/47/29/295203**.

32 C. Kong, J. Gao, J. Zhu, A. Ehn, M. Aldén and Z. Li, Effect of Turbulent Flow on an Atmospheric-Pressure AC Powered Gliding Arc Discharge, *J. Appl. Phys.*, 2018, **123**(22), DOI: **10.1063/1.5026703**.

33 O. Mutaf-Yardimci, A. V. Saveliev, A. A. Fridman and L. A. Kennedy, Thermal and Nonthermal Regimes of Gliding Arc Discharge in Air Flow, *J. Appl. Phys.*, 2000, **87**(4), 1632–1641, DOI: **10.1063/1.372071**.

34 R. Zhang, H. Huang and T. Yang, Mode Transition Induced by Back-Breakdown of the Gliding Arc and Its Influence Factors, *High Volt.*, 2020, **5**(3), 306–312, DOI: **10.1049/hve.2019.0162**.

35 B. S. Patil, F. J. J. Peeters, G. J. van Rooij, J. A. Medrano, F. Gallucci and J. Lang, *et al.*, Plasma Assisted Nitrogen Oxide Production from Air: Using Pulsed Powered Gliding Arc Reactor for a Containerized Plant, *AIChE J.*, 2018, **64**(2), 526–537, DOI: **10.1002/aic.15922**.

36 I. Muzammil, D. H. Lee, D. K. Dinh, H. Kang, S. A. Roh and Y. N. Kim, *et al.*, A Novel Energy Efficient Path for Nitrogen Fixation Using a Non-Thermal Arc, *RSC Adv.*, 2021, **11**(21), 12729–12738, DOI: **10.1039/d1ra01357b**.

37 M. Janda, K. Hensel, Z. Machala and T. A. Field, The Influence of Electric Circuit Parameters on NOx Generation by Transient Spark Discharge, *J. Phys. D: Appl. Phys.*, 2023, **56**(48), DOI: **10.1088/1361-6463/ace634**.

38 E. Vervloessem, M. Aghaei, F. Jardali, N. Hafezkhiabani and A. Bogaerts, Plasma-Based N2Fixation into NOx: Insights from Modeling toward Optimum Yields and Energy Costs in a Gliding Arc Plasmatron, *ACS Sustainable Chem. Eng.*, 2020, **8**(26), 9711–9720, DOI: **10.1021/acssuschemeng.0c01815**.

39 W. Wang, B. Patil, S. Heijkers, V. Hessel and A. Bogaerts, Nitrogen Fixation by Gliding Arc Plasma: Better Insight by Chemical Kinetics Modelling, *ChemSusChem*, 2017, **10**(10), 2145–2157, DOI: **10.1002/cssc.201700095**.

40 M. A. Malik, Nitric Oxide Production by High Voltage Electrical Discharges for Medical Uses: A Review, *Plasma Chem. Plasma Process.*, 2016, **36**(3), 737–766, DOI: **10.1007/s11090-016-9698-1**.

5420 | *Catal. Sci. Technol.*, 2024, **14**, 5405–5421

This journal is © The Royal Society of Chemistry 2024

41 H. Tsukahara, T. Ishida and M. Mayumi, Gas-Phase Oxidation of Nitric Oxide: Chemical Kinetics and Rate Constant, *Nitric Oxide*, 1999, **3**(3), 191–198, DOI: **10.1006/niox.1999.0232**.

42 M. J. Pavlovich, T. Ono, C. Galleher, B. Curtis, D. S. Clark and Z. Machala, *et al.*, Air Spark-like Plasma Source for Antimicrobial NOx Generation, *J. Phys. D: Appl. Phys.*, 2014, **47**(50), DOI: **10.1088/0022-3727/47/50/505202**.

43 V. Ivanov, T. Paunska, S. Lazarova, A. Bogaerts and S. Kolev, Gliding Arc/Glow Discharge for CO2conversion: Comparing the Performance of Different Discharge Configurations, *J. CO2 Util.*, 2023, **67**, 102300, DOI: **10.1016/j.jcou.2022.102300**.

44 M. P. Pradhan and J. B. Joshi, Absorption of NO(x) Gases in Plate Column: Selective Manufacture of Sodium Nitrite, *Chem. Eng. Sci.*, 2000, **55**(7), 1269–1282, DOI: **10.1016/S0009-2509(99)00397-8**.

45 E. C. Neyts, Plasma-Surface Interactions in Plasma Catalysis, *Plasma Chem. Plasma Process.*, 2016, **36**(1), 185–212, DOI: **10.1007/s11090-015-9662-5**.

46 J. Hong, S. Prawer and A. B. Murphy, Plasma Catalysis as an Alternative Route for Ammonia Production: Status, Mechanisms, and Prospects for Progress, *ACS Sustainable Chem. Eng.*, 2018, **6**(1), 15–31, DOI: **10.1021/acssuschemeng.7b02381**.

47 P. Peng, P. Chen, C. Schiappacasse, N. Zhou, E. Anderson and D. Chen, *et al.*, A Review on the Non-Thermal Plasma-Assisted Ammonia Synthesis Technologies, *J. Cleaner Prod.*, 2018, **177**, 597–609, DOI: **10.1016/j.jclepro.2017.12.229**.

48 B. S. Patil, N. Cherkasov, J. Lang, A. O. Ibhadon, V. Hessel and Q. Wang, Low Temperature Plasma-Catalytic NOxsynthesis in a Packed DBD Reactor: Effect of Support Materials and Supported Active Metal Oxides, *Appl. Catal., B*, 2016, **194**, 123–133, DOI: **10.1016/j.apcatb.2016.04.055**.

49 T. Q. Zhang, X. S. Li, J. L. Liu, X. Q. Wen and A. M. Zhu, Plasma Nitrogen Fixation: NOx Synthesis in MnOx/Al2O3 Packed-Bed Dielectric Barrier Discharge, *Plasma Chem.*

50 A. Bogaerts, X. Tu, J. C. Whitehead, G. Centi, L. Lefferts and O. Guaitella, *et al.*, The 2020 Plasma Catalysis Roadmap, *J. Phys. D: Appl. Phys.*, 2020, **53**(44), DOI: **10.1088/1361-6463/ab9048**.

51 P. Atkins and J. De Paula, *Atkins' Physical Chemistry*, Macmillan Higher Education, 2006.

52 F. Jardali, S. Van Alphen, J. Creel, H. Ahmadi Eshtehardi, M. Axelsson and R. Ingels, *et al.*, NOxproduction in a Rotating Gliding Arc Plasma: Potential Avenue for Sustainable Nitrogen Fixation, *Green Chem.*, 2021, **23**(4), 1748–1757, DOI: **10.1039/d0gc03521a**.

53 X. Pei, D. Gidon and D. B. Graves, Specific Energy Cost for Nitrogen Fixation as NOxusing DC Glow Discharge in Air, *J. Phys. D: Appl. Phys.*, 2020, **53**(4), ab5095, DOI: **10.1088/1361-6463/ab5095**.

54 X. Pei, D. Gidon, Y. J. Yang, Z. Xiong and D. B. Graves, Reducing Energy Cost of NOx Production in Air Plasmas, *Chem. Eng. J.*, 2019, **362**, 217–228, DOI: **10.1016/j.cej.2019.01.011**.

55 A. A. Abdelaziz, Y. Teramoto, T. Nozaki and H. H. Kim, Toward Reducing the Energy Cost of NOx Formation in a Spark Discharge Reactor through Pinpointing Its Mechanism, *ACS Sustainable Chem. Eng.*, 2023, **11**(10), 4106–4118, DOI: **10.1021/acssuschemeng.2c06535**.

56 X. Meng, N. Lu and K. Shang, *et al.* Dielectric-Boosted Gliding Arc Discharge for N_2 Fixation into NO_x, *Plasma Chem. Plasma Process.*, 2024, DOI: **10.1007/s11090-024-10474-8**.

57 K. H. R. Rouwenhorst, F. Jardali, A. Bogaerts and L. Lefferts, Erratum: From the Birkeland-Eyde Process towards Energy-Efficient Plasma-Based NOX Synthesis: A Techno-Economic Analysis (Energy Environmental Science (2021) 14 (2520-2534) DOI: 10.1039/D0EE03763J), *Energy Environ. Sci.*, 2023, **16**(12), 6170–6173, DOI: **10.1039/d3ee90066e**.

This journal is © The Royal Society of Chemistry 2024

Catal. Sci. Technol., 2024, **14**, 5405–5421 | **5421**